ACS OMEGA

http://pubs.acs.org/journal/acsodf

Article

Efficient $BiVO_4$-Based Photoanode with Chemically Precipitated Hierarchical Cobalt Borate (Co-B_i) Oxygen Evolution Reaction Catalysts

Ruben Dell'Oro, Maurizio Sansotera, Claudia L. Bianchi, and Luca Magagnin*

Cite This: *ACS Omega* 2023, 8, 20332−20341

Read Online

ACCESS | Metrics & More | Article Recommendations | Supporting Information

ABSTRACT: The integration of cobalt borate OER catalysts with electrodeposited $BiVO_4$-based photoanodes through a simple drop casting technique was shown to provide an improvement of the photoelectrochemical performance of electrodes under simulated solar light. Catalysts were obtained by chemical precipitation mediated by $NaBH_4$ at room temperature. Scanning electron microscopy (SEM) investigation of precipitates showed a hierarchical structure with globular features covered in nanometric thin sheets providing a large active area, whereas X-ray diffraction (XRD) and Raman spectroscopy highlighted their amorphous structure. The photoelectrochemical behavior of samples was investigated by linear scan voltammetry (LSV) and electrochemical impedance spectroscopy (EIS) techniques. The amount of particles loaded onto $BiVO_4$ absorbers was optimized by variation of the drop cast volume. The enhancement of photocurrent generation by Co-B_i-decorated electrodes with respect to bare $BiVO_4$ was observed with an increase from 1.83 to 3.65 mA/cm^2 at 1.23 V vs RHE under AM 1.5 simulated solar light, corresponding to a charge transfer efficiency of 84.6%. The calculated maximum applied bias photon-to-current efficiency (ABPE) value for optimized samples was 1.5% at 0.5 V applied bias. Under constant illumination at 1.23 V vs RHE, a depletion of photoanode performances was observed within an hour, likely due to the detachment of the catalyst from the electrode surface.

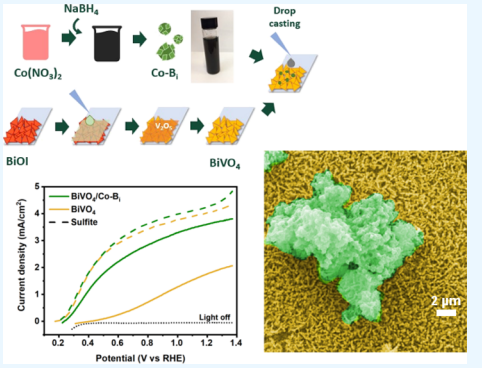

1. INTRODUCTION

The use of hydrogen as a sustainable energy vector through fuel cell technology, as well as its use as an energy storage medium, has been a topic of discussions throughout the last decades as a result of the intrinsic intermittence of renewable power sources. However, most of the hydrogen gas production today still relies on fossil fuels, with high-carbon-footprint processes such as steam reforming, making its use on a large scale not viable yet.[1−4] Among green H_2 synthesis techniques, electrolysis has great potential thanks to the possibility of being supplied by renewable energy sources and having unharmful and abundant substances like H_2O and O_2 as feedstock and byproduct, respectively.[5−7] In particular, photoelectrochemical (PEC) water splitting could be a smart approach to the problem by integrating light converting elements to the electrolytic cell in a compact device.[8,9] Nevertheless, having semiconductors in direct contact to the chemical environment of an electrochemical cell unavoidably introduces limitations arising from the slow kinetics of charge transfer and redox reactions at the electrode/electrolyte interface, as well as from the low stability of the device under long time operation. The most promising approach for PEC cell technology arguably is the tandem configuration, which involves the use of a photoactive material in both electrodes.[10] In this way, the sum of the thermodynamic voltage and the overpotentials of oxygen and hydrogen evolution reactions is overcome by the sum of the two photovoltages, with no external bias applied. In this configuration, photoanodes are mainly made of n-type oxides, with TiO_2,[11−13] WO_3,[14−16] $BiVO_4$,[17−19] and Fe_2O_3[20,21] being the most widely studied, because working in anodic conditions requires materials with good stability against oxidation. Therefore, photoanodes often act as a bottleneck element of the device because, in most cases, semiconductor oxides are characterized by large band gaps that limit the maximum photocurrent produced. Among the candidate materials, bismuth vanadate ($BiVO_4$) has a good combination of properties, namely, a proper band alignment with water oxidation potential, an acceptable band gap width (2.4 eV) that allows a maximum theoretical photocurrent of 7.5 mA/cm^2, and a sufficiently high chemical stability in working conditions.[17,22] On the other hand, high recombination rates and slow kinetics of OER at the $BiVO_4$ surface significantly limit the performance of this material. Several solutions have

Received: January 6, 2023
Accepted: May 8, 2023
Published: May 26, 2023

been explored to avoid these problems through nanostructuring,[23−25] semiconductor doping and defect engineering,[26−28] introduction of heterojunctions for charge separation interfaces,[29−31] and the implementation of a co-catalyst on the surface of the electrode. Catalysts play a fundamental role in reducing the activation energy for the several steps involved in the water oxidation reaction but also favor a rapid charge extraction from the absorber material, avoiding recombination phenomena as well as photoinduced corrosion.[32,33] Well-known and efficient catalysts for OER are IrO_2 and RuO_2, which are hardly suitable for a scalable technology because of the high cost and scarcity.[33,34] For this reason, the investigation of cheaper and earth-abundant alternatives found some valid candidates in oxides, hydroxides, and oxyhydroxides of transition metals, namely, Mn, Fe, Ni, and Co,[35−40] with particularly high performances in the case of the combination of more than one metallic element.[18,41−43] Moreover, non-oxide materials such as phosphates,[43,44] sulfides,[45,46] and borates/borides[47−49] have shown catalytic activity thanks to the formation of oxide/hydroxide domains, which act as active sites for the adsorption and reaction of OER intermediate species.[50] Boron-based co-catalysts are gaining interest due to their performance and affinity to the commonly used mild alkaline potassium borate buffer solution for photoanode testing. Many works show this class of materials to provide several active sites thanks to an amorphous structure or good combination of crystalline and amorphous domains.[50,51] Implementation of transition metal borates/borides in either dark or light driven electrolysis is reported through different synthesis methods, including solid-state reactions,[51] electrochemical deposition processes,[52−56] and chemical precipitation.[48,57−59] In the latter case, the formation of micro- to nanosized particles has been obtained by the interaction of Co^{2+}, Ni^{2+}, or Fe^{3+} ions with the $NaBH_4$ hydrolysis products, inducing the precipitation of metal borides or borates depending on deposition conditions.[47] Therefore, with a very simple room temperature reaction, for example, cobalt borate (Co-B_i) nanosheet structures can be easily obtained by precipitation, a providing large effective area for faster OER and reduced overpotentials.[57,60] In addition, this kind of synthesis by precipitation allowed the combination of borate catalysts with conductive nanostructured materials, such as carbon nanotubes,[51] graphene,[61] carbon black particles,[62] or MXenes.[60] This approach proved to be a promising strategy to improve the performances of electrodes. Considering PEC water splitting, more commonly, $BiVO_4$ photoanodes with a thin conformal layer of a borate-based catalyst (mainly obtained by electrochemical processes) have shown significantly enhanced photocurrents due to an improved charge extraction and OER kinetics.[52,53,63,64]

In this work, a simple integration approach of precipitated hierarchical Co-B_i particle catalysts on the $BiVO_4$ photoelectrode by drop casting is proposed. Amorphous globular Co-B_i particles with nanometric sheets on the surface were obtained and dispersed in ethanol for the application on $BiVO_4$. The achieved photoanode showed an improvement of the photogenerated current that almost doubled from 1.83 to 3.65 mA/cm^2 at 1.23 V vs RHE with respect to the bare electrode, with a maximum applied bias to photocurrent efficiency (ABPE) reaching 1.5% with 0.5 V external voltage applied.

2. EXPERIMENTAL METHODS

2.1. $BiVO_4$ Synthesis. $BiVO_4$ was synthesized according to a widely reported procedure[18] of electrodeposition of a BiOI precursor and thermal conversion. An electrodeposition solution was prepared by dissolving 0.4 M KI (Sigma Aldrich, >99.5%) in 50 mL of deionized water (DIW). pH was adjusted to 1.7 with HNO_3, and then finely ground 0.04 M $Bi(NO_3)_3$ (Sigma Aldrich, 98%) was added. Under vigorous stirring, 0.23 M *p*-benzoquinone (Sigma Aldrich, >98%) in 20 mL of ethanol was poured in the previous solution and then kept stirring for several minutes. FTO (fluorine-doped tin oxide) coated glass (Sigma Aldrich, ∼7 Ω/sq) substrates were prepared by sequential ultrasonic cleaning in 10 g/L ALCONOX aqueous solution and ethanol for 5 min each step. BiOI electrodeposition was performed with a three-electrode cell using a FTO substrate as working electrode (WE), Ag/AgCl (3 M KCl) reference electrode (RE), and a Pt-coated titanium net as counter electrode (CE). The deposition was carried out in potentiostatic condition, with an AMEL 2550 potentiostat, applying −0.1 V vs Ag/AgCl to the WE for approximately 2−3 min, the time required for a 0.13 C cm^{-2} charge density to pass through the electrode. Prior to the thermal conversion, 30 μL cm^{-2} of DMSO solution containing 0.2 M vanadyl acetylacetonate (VO-$(acac)_2$) (Sigma Aldrich, 98%) was drop cast onto the BiOI precursor. Successively, samples were kept in a desiccator at 70 °C until completely dry. A thermal annealing to convert BiOI to $BiVO_4$ was performed in air with a tubular furnace with a heating ramp of 2 °C min^{-1} to 450 °C, which was maintained for 120 min and then cooled naturally. Eventually, excess V_2O_5 formed on the $BiVO_4$ surface was removed by a 30 min etching in 1 M NaOH solution.

2.2. Co-B_i Synthesis and Electrode Preparation. The Co-B_i powder was obtained through a modified precipitation technique.[60,61] In a beaker, 291 mg of $Co(NO_3)_2$ hexahydrate (Alfa Aesar, >98%) was dissolved in DIW by sonication. To initiate the precipitation, 5 mL of 0.5 M $NaBH_4$ aqueous solution was poured in the beaker with fast stirring. $NaBH_4$ reacted quickly with gas evolution. The solution was kept stirring for 40 min, and then the precipitate was rinsed and centrifuged several times with DIW and then ethanol to remove residues of the reaction solution. Eventually, the powder was dried from ethanol in a desiccator at 35 °C.

Co-B_i was deposited as catalysts onto the $BiVO_4$ photoanode surface by drop casting an ethanol dispersion of the powder (0.5 mg/mL) obtained by 15 min sonication. The catalyst loading was varied by changing the dropped volume (10, 25, and 50 μL/cm^2). After application of the dispersion with a micropipette, ethanol was evaporated in the desiccator.

2.3. Material Characterization. Scanning electron microscopy (SEM) imaging of powders and electrodes was performed with a Zeiss EVO 50 EP microscope provided of electron dispersive spectroscopy (EDS) (Oxford Instruments INCA x-sight detector). X-ray diffraction and Raman spectroscopy were carried out with a Malvern Panalytical Empyrean ($K\alpha 1_{Cu}$ = 1.54058 Å) and LABRAM HR 800 UV HORIBA JOBIN YVON (532 nm laser wavelength), respectively. X-ray photoelectron spectroscopy spectra were obtained by using an M-probe apparatus (Surface Science Instruments). The source was monochromatic Al Kα radiation (1486.6 eV). A spot size of 200 × 750 μm and pass energy of 25 eV were used. For high-resolution spectra, the 1s level of

https://doi.org/10.1021/acsomega.3c00104
ACS Omega 2023, 8, 20332−20341

hydrocarbon-contaminant carbon was taken as the internal reference at 284.6 eV. For each sample, survey analyses in the whole range of the X-ray spectrum were performed to determine the surface elemental composition. Similarly, high-resolution scans in the regions of C 1s, O 1s, Co $2p_{3/2}$, and B 1s were acquired for the determination of the chemical environment surrounding every species.

2.4. Photoelectrochemical Measurements. The photoelectrochemical behavior of samples was evaluated with linear scan voltammetry (LSV) in a three-electrode configuration comprising $BiVO_4$ photoanodes as WE, Ag/AgCl (3 M KCl) RE, and platinum-coated titanium mesh as CE performed with an AMEL 2559 potentiostat. The electrolyte used for photoelectrical characterization was a 0.5 M potassium borate buffer (pH 9.5). Tests were also performed in 0.5 M borate buffer with 0.5 M Na_2SO_3 acting as the hole scavenger. Measurements were carried out under 0.1 W/cm^2 AM 1.5 light of an ABET Sunlite 11002 solar simulator Xe arc lamp. The curves were reported after conversion of potential values versus reversible hydrogen electrode (RHE) according to the Nernst equation. LSV curves were measured in two-electrode configuration using only Pt mesh as CE for the calculation of ABPE through the formula in the Supporting Information. Electrochemical impedance spectroscopy (EIS) was performed in the same three-electrode configuration with an Admiral Squidstat Plus with an AC potential with 10 mV amplitude oscillating at 0.3 V vs RHE in the 100 mHz−1 MHz range.

3. RESULTS AND DISCUSSION

Cobalt borate (Co-B_i) OER catalysts were precipitated from a $Co(NO_3)_2$ solution by addition of $NaBH_4$. According to previous reports,[47,65] metallic ion reduction with sodium borohydride exploits the spontaneous hydrolysis reaction borohydride (1), which first induces the formation of cobalt borides (Co-B) that are good catalyzers of further dissociation of $NaBH_4$ (2). Thanks to the formation of borate groups $(BO_2)^-$, $Co(BO_2)_2$ cobalt borate is formed (Co-B_i) (3).

$$2Co^{2+}_{(aq)} + 4BH_4^-{}_{(aq)} + 9H_2O_{(l)} \rightarrow Co_2B_{(s)} + 12.5H_{2(g)} + 3B(OH)_{3(aq)} \quad (1)$$

$$NaBH_{4(aq)} + 2H_2O_{(l)} \xrightarrow{Co_2B} 4H_{2(g)} + NaBO_{2(aq)} \quad (2)$$

$$Co^{2+}_{(aq)} + 2NaBO_{2(aq)} \rightarrow 2Na^+_{(aq)} + Co(BO_2)_{2(s)} \quad (3)$$

Different synthesis outcomes can be obtained from this system, i.e., borides, borates, or metallic cobalt, as well as hybrid structures and nonstoichiometric compounds, depending on the following reaction parameters: reactants' order of addition, reaction atmosphere (air/inert), reaction time, and BH_4^-/Co^{2+} ratio.[65−67] Here, rapid addition of a small volume of concentrated $NaBH_4$ to a cobalt containing solution (B/Co = 2.5 in the reaction mixture) was performed followed by several minutes of stirring in air, according to reported works showing hierarchical Co-B_i nanosheets as the main outcome.[60−62] The formation of 2D structures was shown to be favored by the use of nitrates as Co precursors.[68]

Centrifugation and drying of the precipitate led to a dark brown powder. SEM micrographs of the powder (Figure 1) indicate the formation of clusters of few micrometers in size constituted of globular features. The surface of the particles is characterized by nanometric thin sheets that increase the overall active area with a hierarchical structure, which is beneficial to the catalytic performance because more active sites are available for the OER reaction.

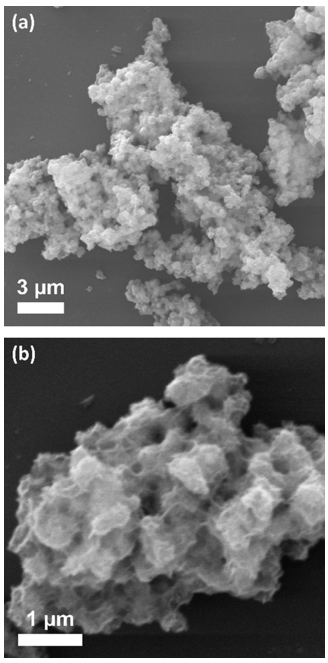

Figure 1. SEM micrographs of Co-B_i hierarchical particles at different magnifications (a, b).

To determine the structure of the material composing the precipitate, XRD analysis was performed (Figure 2a). In confirmation of reported results for similar syntheses, no characteristic peaks were observed, implying that an

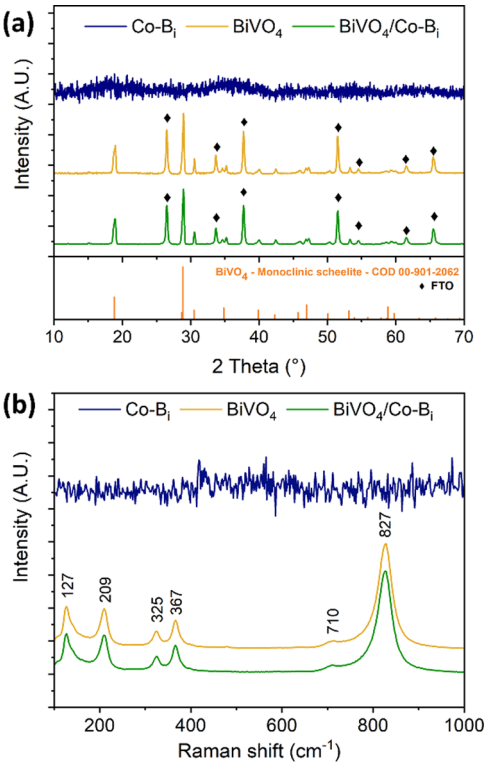

Figure 2. XRD spectra of Co-B_i powders and $BiVO_4$ (a) and the corresponding Raman spectra (b).

https://doi.org/10.1021/acsomega.3c00104
ACS Omega 2023, 8, 20332−20341

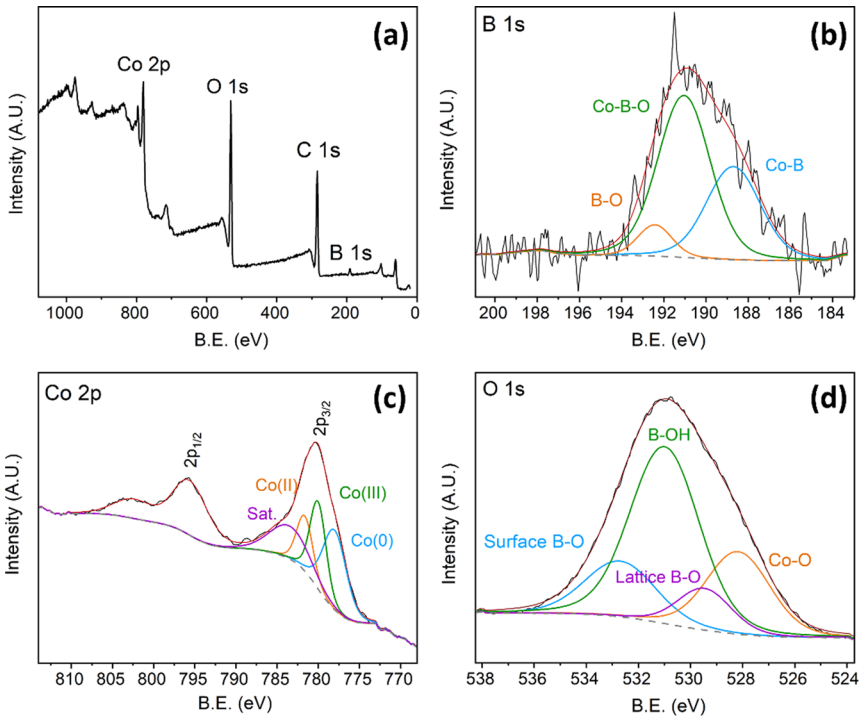

Figure 3. XPS analysis of Co-B_i catalysts. Survey (a) and high-resolution scans and deconvolution of B 1s (b), Co 2p (c), and O 1s (d).

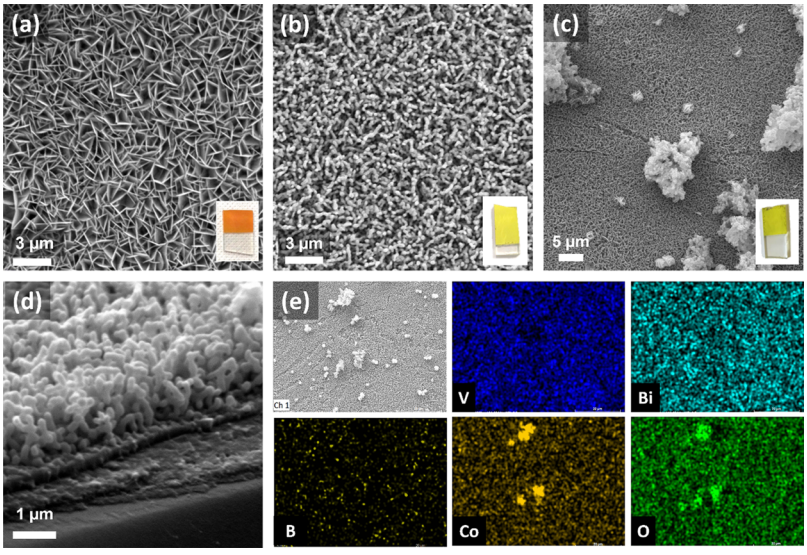

Figure 4. SEM micrographs and relative digital photos: BiOI (a), $BiVO_4$ (b), and $BiVO_4$/Co-B_i (c). Cross-sectional SEM image of a $BiVO_4$ nanostructured film (d). EDS mapping of Co-B_i decorated $BiVO_4$ (e).

amorphous structure of the cobalt-boron based material was obtained. The Raman (Figure 2b) spectrum confirmed the absence of structural order, not showing a significant signal in the analyzed wavenumber range.

X-ray photoelectron spectroscopy (XPS) was then performed to gain information on the composition and chemical state of elements composing the particulate surface. The survey analysis showed the presence of Co, B, and O in the material (Figure 3a), with an atomic composition expressed by the ratio Co/B/O of 1.8:1:6. High-resolution scans on the elements' main peak highlighted several components because of the nonstoichiometric composition of the material. Considering the 1s peak of boron (Figure 3b), two components related to B bound to O are individuated at 191.0 and 192.4 eV, and they can be associated to Co−B−O and B−O bonds of cobalt borate, respectively. In addition, a third contributor at lower binding energy (188.7 eV) might be associated to the presence of cobalt boride (Co-B) domains in the particles. Considering the signal related to Co $2p_{3/2}$ (Figure 3c), its deconvolution indicated three components related to different cobalt oxidation states, namely, Co(II), Co(III), and Co(0) at 781.6, 780.0, and 778.0 eV, respectively. The peak related to metallic Co was associated to the formation of boride phases along with borate, corresponding to higher oxidation states.[47,69] A typical satellite peak is then observed at 783.4 eV. Eventually, the analysis of O 1s signal (Figure 3d) showed contribution from boron-bound oxygen, separated in three main components associated to the surface oxygen (532.7 eV),

https://doi.org/10.1021/acsomega.3c00104
ACS Omega 2023, 8, 20332−20341

hydroxyl groups (531.0 eV), and lattice oxygen (529.5 eV).[47,57,70] An additional peak at lower binding energy is observed at 528.2 eV, which might indicate the formation of Co−O bonds related to superficial oxide/hydroxide domains.

$BiVO_4$ absorber films were synthesized according to a typical electrochemical method, first depositing a BiOI nanosheet layer by electrodeposition, shown in the SEM micrograph (Figure 4a). The calcination treatment allowed the conversion of the film into the typical nanoporous $BiVO_4$ layer (Figure 4b), with 200−300 nm wormlike structures, providing a large surface area and a sufficiently short path for charge carriers from the bulk to the surface of the semiconductor. From the cross-sectional image of $BiVO_4$ the thickness of the semiconductor layer appeared to be approximately 1 μm (Figure 4d). As reported in Figure 2a, the complete monoclinic scheelite pattern with main characteristic peaks at 18.97, 28.95, and 30.55° in the XRD spectrum of the $BiVO_4$ film confirmed that nanostructures feature randomly oriented crystallites.

Similarly, the Raman spectrum of the semiconductor (Figure 2b) showed characteristic bands of $BiVO_4$ at 127, 209, 325, 367, and 827 cm^{-1}. No significant variation of XRD and Raman spectra is observed upon deposition of Co-B_i on $BiVO_4$. The application of the catalyst on the surface of the photoanode was obtained with a very simple drop casting process. Different volumes of the dispersion (10, 25, and 50 $\mu L/cm^2$) were cast on $BiVO_4$ to observe the effect of different catalyst loadings on the surface on the photoelectrochemical performance of the photoanode. Figure 5 shows a schematic

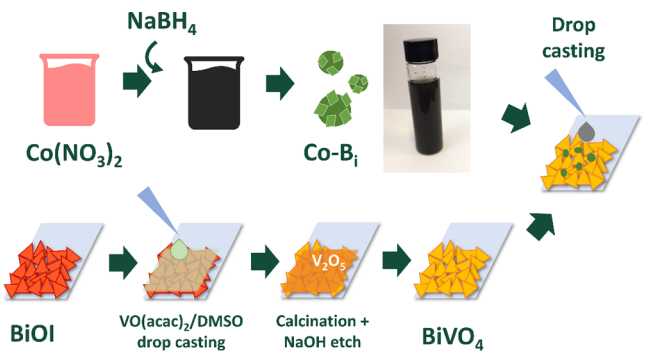

Figure 5. Schematic representation of the photoanode fabrication route.

representation of the overall process of electrode fabrication. SEM micrographs of the decorated electrode show Co-B_i particles distributed on the surface of the nanoporous layer (Figure 4c), lying above the nanometric features of $BiVO_4$. EDS mapping allows one to distinguish Co-B_i catalysts (Figure 4e), indicated by more intense spots in the Co and O distribution, from smaller particles, which are $BiVO_4$ clusters grown on top of the main layer, as already observed in other works.[19] The weak and delocalized signal in the B map should be related to the scarce sensitivity of the instrument to boron, the lightest detectable element, which is below the detectability threshold in the EDS spectrum of Co-B_i particles (Figure S1). The distribution of catalysts is random, and their number per unit area increases with the drop cast volume (Figure 6a−c). In any case, in the considered areas, no interaction between particles or clustering is observed with higher catalyst loading. The large size of catalysts with respect to the nanometric structures of the $BiVO_4$ film can suggest that improvements in the photoanode performance could be achieved, increasing both the contact area with the catalyst and surface coverage.

A better interaction between the absorber material and catalyst may be expected with a reduced size of Co-B_i particles, allowing them to deposit in the porosities of the semiconductor, for a better exploitation of the large $BiVO_4$ area. Ultrasonication with a probe sonicator was investigated to break catalysts into smaller particles, but a reduction in the photocurrent produced at low applied bias was observed (Figure S2). This does not exclude that a distribution of nanometric particles or aggregates, produced through alternative methods to drop casting, can be beneficial.

Regardless of the previous statements, in the presence of Co-B_i, a significant improvement of the photoelectrochemical performance, with respect to the bare $BiVO_4$, was observed with LSV testing under illumination. The best photocurrent yield was obtained with an intermediate amount of catalyst (25 $\mu L/cm^2$) deposited on the surface of the electrode (Figure 6d). An important increase in photocurrent density was observed at low applied bias, overcoming 1 mA/cm^2 at 0.38 V vs RHE, and the onset potential almost coincided with the one measured in the presence of the Na_2SO_3 hole scavenger, proving the high catalytic activity of Co-B_i (Figure 7a). Dark current density curves are shown in the plot, measuring nearly null current for the entire scan, indicating that the current density under illumination was all generated by light conversion. Considering the photocurrent value at 1.23 V vs RHE, a large enhancement is obtained, with an increase from 1.83 mA/cm^2 for the bare BiVO4 electrode to 3.65 mA/cm^2 in the case of the optimized catalyst-decorated sample. The improved charge transfer kinetics at the electrode/electrolyte thanks to Co-B_i was confirmed by electrochemical impedance spectroscopy (EIS) measurements (Figure 7b): Nyquist plots showed the recognizable semicircular graphs, indicating that the electrode behavior could be modelized with the Randles equivalent circuit reported in the inset, featuring electrolyte resistance (R_s), charge transfer resistance (R_{ct}), and a constant phase capacitive element (CPE) (fitting parameters are reported in Table S1).[64,71,72] The reduced diameter in the presence of catalysts indicated a reduction of the charge transfer resistance at the surface. The charge transfer resistances (R_{ct}'s) obtained from the plot fitting were 33.67 and 3.70 kΩ for pristine and catalyst-decorated $BiVO_4$, respectively. The charge transfer efficiency of photoanodes reported in Figure 7c was calculated as the ratio between photocurrent densities measured without and with the Na_2SO_3 hole scavenger, with the latter being an indication of the maximum electrical output of the electrode in ideal charge transfer conditions through the electrode surface. Starting from a 44.8% efficiency at 1.23 V vs RHE of the bare $BiVO_4$ material, Co-B_i particles allowed the achievement of the remarkable value of 84.6%. It is worth noticing that the LSV curve in the presence of sulfite after catalyst deposition was almost identical to the reference sample (Figure 7a), indicating no current generation contribute was provided by Co-B_i, whereas the performance improvement was entirely related to a favored oxygen evolution. Similarly, a higher overall efficiency with the catalysts was evaluated by ABPE calculation from LSV measurements carried out in two-electrode conditions using a Pt mesh as nonphotoactive cathode. In fact, the ABPE maximum of the Co-B_i decorated sample was 5 times higher than that of the reference sample, reaching 1.5%, which is comparable to state-of-art performances of $BiVO_4$-based photoanodes with OER catalysts (Figure 6d). In particular,

https://doi.org/10.1021/acsomega.3c00104
ACS Omega 2023, 8, 20332−20341

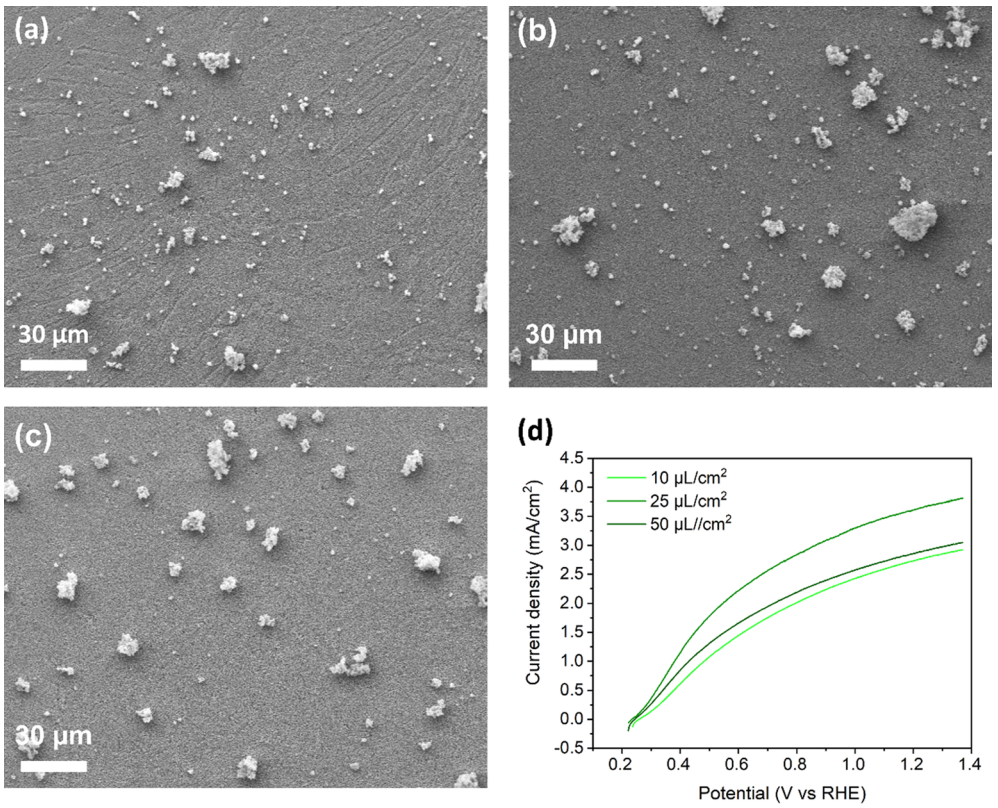

Figure 6. Representative SEM micrographs of $BiVO_4$ decorated with different drop cast volumes of catalyst dispersion: 10 μL/cm^2 (a), 25 μL/cm^2 (b), and 50 μL/cm^2 (c). Dependence on the drop cast volume of catalyst dispersion of LSV curves of $BiVO_4$/Co-B_i in 1 M potassium borate (pH 9.5) under 100 mW/cm^2 AM 1.5 light (d).

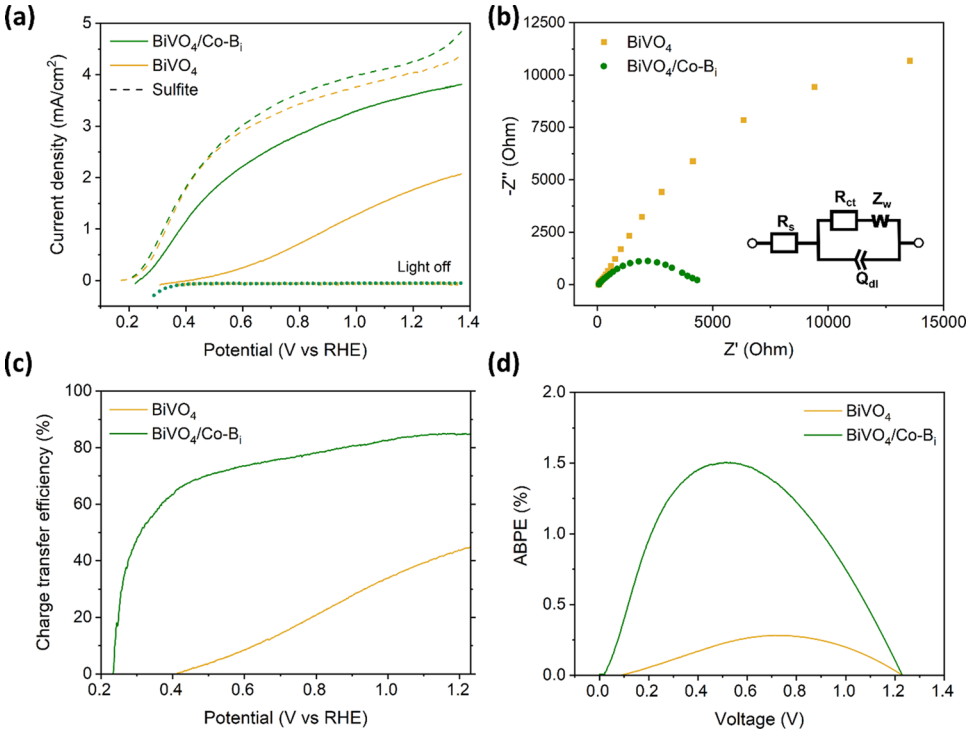

Figure 7. Photoelectrochemical characterization of $BiVO_4$ photoanodes. (a) LSV test in 1 M potassium borate (pH 9.5) under AM 1.5 light with (dashed line) and without (solid line) Na_2SO_3 hole scavenger. (b) Electrochemical impedance spectroscopy Nyquist plots with Randles equivalent circuit scheme. (c) Charge transfer efficiency (η_{ct}). (d) Applied bias photon-to-current efficiency (ABPE).

the half-cell efficiency is higher than that for a comparable Co-B_i/$BiVO_4$ photoanode proposed by Xue et al., with electrochemically deposited cobalt borate, showing a maximum ABPE lower than 1% (2.5 mA/cm^2 at 1.23 V vs RHE), which was

https://doi.org/10.1021/acsomega.3c00104
ACS Omega 2023, 8, 20332−20341

increased to about 1.3% only by the introduction of an ultrathin TiO_2 layer between the photoabsorber and co-catalyst (Co-Bi/TiO_2/$BiVO_4$) for a better charge transfer.[56] Noteworthily, the maximum efficiency shifted towards a lower applied bias value (0.5 V vs RHE) with Co-B_i (Figure 6d), in accordance with the higher current density yield. This is a desirable result in the perspective of the integration of the photoanode in a tandem device because the cell's working point usually occurs close to the onset points of the two electrodes, so having higher efficiency at lower applied bias would provide a better overall performance.

Eventually, the durability of the photoanodes and catalyst was evaluated by measuring the photocurrent density produced while maintaining the sample exposed to the simulated solar radiation for 2 h under a constant applied potential, 1.23 V vs RHE (Figure 8). According to the chronoamperometry, the

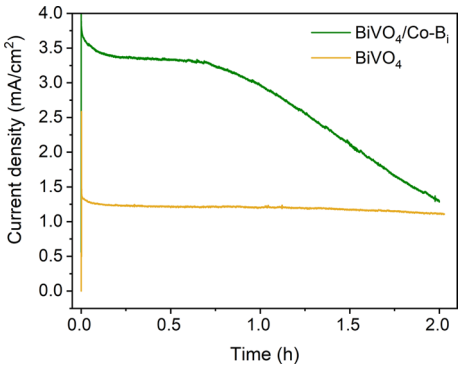

Figure 8. Chronoamperometric analyses of bare and Co-B_i-decorated $BiVO_4$ under AM 1.5 simulated solar light at 1.23 V vs RHE.

Co-B_i-decorated sample maintained the initial electrical output for almost 45 min. However, after that first interval, performance started to decrease monotonically, reaching the photocurrent value of the $BiVO_4$ photoanode 2 h after the beginning of the test. To investigate the phenomena producing the performance degradation, SEM analysis on the sample after chronoamperometry was performed. Degradation of either $BiVO_4$ or Co-B_i could be expected to induce such a change in the electrode behavior. However, no significant modification of the microstructure that may indicate $BiVO_4$ dissolution or degradation was observed after exposure to working conditions (Figure S3), as it could be expected according to literature reports about photodegradation of the semiconductor in borate-based electrolytes.[73] Moreover, a similar reduction in photocurrent may be expected in the bare $BiVO_4$ electrode, which is not the case. Similarly, high magnification of the catalyst particle still showed the characteristic nanosheets covering the surface, which seemed to exclude a reduction or depletion of the catalyst surface. Representative images of the electrode surface at lower magnification before and after a long exposure test were compared in Figure S4. A reduction of the number of catalyst particles distributed on the semiconductor could be observed (Figure S5), which led to the conclusion that the efficiency reduction might be induced by the detachment of catalyst particles from the surface of the material.

Clearly, toward a reliable application of the presented strategy to improve the performances of $BiVO_4$ photoanodes, this issue should be faced in future work. Adhesion of the catalyst could be improved by reducing the average size of particles, either tailoring the synthesis reaction or introducing a successive treatment (e.g., ball milling), so that a better mechanical interlocking with the $BiVO_4$ nanostructures can be achieved. Also, the use of a binder such as Nafion particles might be viable solution, as proposed for the decoration of electrodes for electrochemical water splitting.[60] Eventually, the introduction of thin conformal layers of TiO_2, as proposed by Xue et al.,[56] should be considered because it may combine the better Co-B_i adhesion to the improved charge transfer reported as well as protection of active materials from photocorrosion phenomena.

4. CONCLUSIONS

Drop casting of micrometric cobalt borate (Co-B_i) OER catalysts on $BiVO_4$ was demonstrated to be a simple yet effective technique for a high-performing photoanode for water splitting. Catalysts with a hierarchical structure consisting in globular features covered in nanometric sheets were synthesized by chemical precipitation at room temperature through reduction of cobalt ions with $NaBH_4$. Photoanodes with good photoelectrochemical behavior were achieved with optimized catalyst loading, producing significant photocurrent density at low applied bias. The photocurrent yield at 1.23 V vs RHE (3.65 mA/cm^2) was doubled with respect to the bare $BiVO_4$ material, and a maximum 1.5% ABPE was achieved at 0.5 V vs RHE. The stability under working conditions of the electrode was observed within an hour with a following drop of performance, probably due to catalyst detachment. Further investigation of the effect of a reduced size of catalyst could be considered a viable pathway toward better results, as an improved interaction of particles with nanometric features of electrodeposited $BiVO_4$ might enhance both the electrical behavior of the photoanode and catalyst adhesion on its surface.

■ ASSOCIATED CONTENT

Supporting Information

The Supporting Information is available free of charge at https://pubs.acs.org/doi/10.1021/acsomega.3c00104.

EDS spectrum of Co-B_i powders; LSV tests before and after sonication of Co-B_i dispersion in ethanol with a probe sonicator; SEM micrographs of $BiVO_4$/Co-B_i before and after long exposure chronoamperometry; and ABPE calculation (PDF)

■ AUTHOR INFORMATION

Corresponding Author

Luca Magagnin − *Department of Chemistry, Materials and Chemical Engineering Giulio Natta, Politecnico di Milano, 20131 Milano, Italy*; orcid.org/0000-0001-5553-6441; Email: luca.magagnin@polimi.it

Authors

Ruben Dell'Oro − *Department of Chemistry, Materials and Chemical Engineering Giulio Natta, Politecnico di Milano, 20131 Milano, Italy*

Maurizio Sansotera − *Department of Chemistry, Materials and Chemical Engineering Giulio Natta, Politecnico di Milano, 20131 Milano, Italy*

Claudia L. Bianchi − *Department of Chemistry, Università degli Studi di Milano, 20133 Milano, Italy*

Complete contact information is available at:

https://doi.org/10.1021/acsomega.3c00104
ACS Omega 2023, 8, 20332−20341

https://pubs.acs.org/10.1021/acsomega.3c00104

Notes

The authors declare no competing financial interest.

■ ACKNOWLEDGMENTS

The authors acknowledge Dott. Manuela Gilberti for performing the XPS analysis at the Università degli Studi di Milano.

■ REFERENCES

(1) Kovač, A.; Paranos, M.; Marciuš, D. Hydrogen in Energy Transition: A Review. *Int. J. Hydrogen Energy* **2021**, *46*, 10016−10035.
(2) Zhang, F.; Zhao, P.; Niu, M.; Maddy, J. The Survey of Key Technologies in Hydrogen Energy Storage. *Int. J. Hydrogen Energy* **2016**, *41*, 14535−14552.
(3) Alamri, B. R.; Alamri, A. R. Technical Review of Energy Storage Technologies When Integrated with Intermittent Renewable Energy. In *1st International Conference on Sustainable Power Generation and Supply, SUPERGEN '09*; IEEE 2009. DOI: 10.1109/SUPERGEN.2009.5348055.
(4) Nikolaidis, P.; Poullikkas, A. A Comparative Overview of Hydrogen Production Processes. *Renewable Sustainable Energy Rev.* **2017**, *67*, 597−611.
(5) Grimm, A.; de Jong, W. A.; Kramer, G. J. Renewable Hydrogen Production: A Techno-Economic Comparison of Photoelectrochemical Cells and Photovoltaic-Electrolysis. *Int. J. Hydrogen Energy* **2020**, *45*, 22545−22555.
(6) Shiva Kumar, S.; Himabindu, V. Hydrogen Production by PEM Water Electrolysis − A Review. *Mater. Sci. Energy Technol.* **2019**, *2*, 442−454.
(7) Grigoriev, S. A.; Fateev, V. N.; Bessarabov, D. G.; Millet, P. Current Status, Research Trends, and Challenges in Water Electrolysis Science and Technology. *Int. J. Hydrogen Energy* **2020**, *45*, 26036−26058.
(8) Kim, J. H.; Hansora, D.; Sharma, P.; Jang, J. W.; Lee, J. S. Toward Practical Solar Hydrogen Production-an Artificial Photosynthetic Leaf-to-Farm Challenge. *Chem. Soc. Rev.* **2019**, *48*, 1908−1971.
(9) Hisatomi, T.; Kubota, J.; Domen, K. Recent Advances in Semiconductors for Photocatalytic and Photoelectrochemical Water Splitting. *Chem. Soc. Rev.* **2014**, *43*, 7520−7535.
(10) Ahmed, M.; Dincer, I. A Review on Photoelectrochemical Hydrogen Production Systems: Challenges and Future Directions. *Int. J. Hydrogen Energy* **2019**, *44*, 2474−2507.
(11) Cho, I. S.; Lee, C. H.; Feng, Y.; Logar, M.; Rao, P. M.; Cai, L.; Kim, D. R.; Sinclair, R.; Zheng, X. Codoping Titanium Dioxide Nanowires with Tungsten and Carbon for Enhanced Photoelectrochemical Performance. *Nat. Commun.* **2013**, *4*, 1723.
(12) Fujishima, A.; Honda, K. Electrochemical Photolysis of Water at a Semiconductor Electrode. *Nature* **1972**, *238*, 37−38.
(13) Ai, G.; Mo, R.; Li, H.; Zhong, J. Cobalt Phosphate Modified TiO_2 Nanowire Arrays as Co-Catalysts for Solar Water Splitting. *Nanoscale* **2015**, *7*, 6722−6728.
(14) Sarnowska, M.; Bienkowski, K.; Barczuk, P. J.; Solarska, R.; Augustynski, J. Highly Efficient and Stable Solar Water Splitting at (Na)WO_3 Photoanodes in Acidic Electrolyte Assisted by Non-Noble Metal Oxygen Evolution Catalyst. *Adv. Energy Mater.* **2016**, *6*, 1600526.
(15) Li, Y.; Mei, Q.; Liu, Z.; Hu, X.; Zhou, Z.; Huang, J.; Bai, B.; Liu, H.; Ding, F.; Wang, Q. Fluorine-Doped Iron Oxyhydroxide Cocatalyst: Promotion on the WO3 Photoanode Conducted Photoelectrochemical Water Splitting. *Appl. Catal., B* **2022**, *304*, No. 120995.
(16) Shin, S.; Han, H. S.; Kim, J. S.; Park, I. J.; Lee, M. H.; Hong, K. S.; Cho, I. S. A Tree-like Nanoporous WO_3 Photoanode with Enhanced Charge Transport Efficiency for Photoelectrochemical Water Oxidation. *J. Mater. Chem. A* **2015**, *3*, 12920−12926.
(17) Kim, J. H.; Lee, J. S. Elaborately Modified $BiVO_4$ Photoanodes for Solar Water Splitting. *Adv. Mater.* **2019**, *31*, 1806938.
(18) Kim, T. W.; Choi, K. S. Nanoporous $BiVO_4$ Photoanodes with Dual-Layer Oxygen Evolution Catalysts for Solar Water Splitting. *Science (80-.).* **2014**, *343*, 990−994.
(19) Kuang, Y.; Jia, Q.; Nishiyama, H.; Yamada, T.; Kudo, A.; Domen, K. A Front-Illuminated Nanostructured Transparent $BiVO_4$ Photoanode for >2% Efficient Water Splitting. *Adv. Energy Mater.* **2016**, *6*, 1501645.
(20) Xie, J.; Yang, P.; Liang, X.; Xiong, J. Self-Improvement of Ti:Fe_2O_3 Photoanodes: Photoelectrocatalysis Improvement after Long-Term Stability Testing in Alkaline Electrolyte. *ACS Appl. Energy Mater.* **2018**, *1*, 2769−2775.
(21) Kim, J. Y.; Magesh, G.; Youn, D. H.; Jang, J.-W.; Kubota, J.; Domen, K.; Lee, J. S. Single-Crystalline, Wormlike Hematite Photoanodes for Efficient Solar Water Splitting. *Sci. Rep.* **2013**, *3*, 2681.
(22) Toma, F. M.; Cooper, J. K.; Kunzelmann, V.; McDowell, M. T.; Yu, J.; Larson, D. M.; Borys, N. J.; Abelyan, C.; Beeman, J. W.; Yu, K. M.; Yang, J.; Chen, L.; Shaner, M. R.; Spurgeon, J.; Houle, F. A.; Persson, K. A.; Sharp, I. D. Mechanistic Insights into Chemical and Photochemical Transformations of Bismuth Vanadate Photoanodes. *Nat. Commun.* **2016**, *7*, 12012.
(23) McDonald, K. J.; Choi, K. S. A New Electrochemical Synthesis Route for a BiOI Electrode and Its Conversion to a Highly Efficient Porous $BiVO_4$ Photoanode for Solar Water Oxidation. *Energy Environ. Sci.* **2012**, *5*, 8553−8557.
(24) Han, H. S.; Shin, S.; Kim, D. H.; Park, I. J.; Kim, J. S.; Huang, P. S.; Lee, J. K.; Cho, I. S.; Zheng, X. Boosting the Solar Water Oxidation Performance of a $BiVO_4$ Photoanode by Crystallographic Orientation Control. *Energy Environ. Sci.* **2018**, *11*, 1299−1306.
(25) Nair, V.; Perkins, C. L.; Lin, Q.; Law, M. Textured Nanoporous Mo:$BiVO_4$ Photoanodes with High Charge Transport and Charge Transfer Quantum Efficiencies for Oxygen Evolution. *Energy Environ. Sci.* **2016**, *9*, 1412−1429.
(26) Kim, T. W.; Ping, Y.; Galli, G. A.; Choi, K. S. Simultaneous Enhancements in Photon Absorption and Charge Transport of Bismuth Vanadate Photoanodes for Solar Water Splitting. *Nat. Commun.* **2015**, *6*, 8769.
(27) Byun, S.; Jung, G.; Moon, S. Y.; Kim, B.; Park, J. Y.; Jeon, S.; Nam, S. W.; Shin, B. Compositional Engineering of Solution-Processed BiVO4 Photoanodes toward Highly Efficient Photoelectrochemical Water Oxidation. *Nano Energy* **2018**, *43*, 244−252.
(28) Wang, S.; He, T.; Chen, P.; Du, A.; Ostrikov, K. (. K.).; Huang, W.; Wang, L. In Situ Formation of Oxygen Vacancies Achieving Near-Complete Charge Separation in Planar $BiVO_4$ Photoanodes. *Adv. Mater.* **2020**, *32*, 2001385.
(29) Baek, J. H.; Kim, B. J.; Han, G. S.; Hwang, S. W.; Kim, D. R.; Cho, I. S.; Jung, H. S. $BiVO_4/WO_3/SnO_2$ Double-Heterojunction Photoanode with Enhanced Charge Separation and Visible-Transparency for Bias-Free Solar Water-Splitting with a Perovskite Solar Cell. *ACS Appl. Mater. Interfaces* **2017**, *9*, 1479−1487.
(30) Lee, D. K.; Choi, K. S. Enhancing Long-Term Photostability of BiVO4 Photoanodes for Solar Water Splitting by Tuning Electrolyte Composition. *Nat. Energy* **2018**, *3*, 53−60.
(31) Pihosh, Y.; Turkevych, I.; Mawatari, K.; Uemura, J.; Kazoe, Y.; Kosar, S.; Makita, K.; Sugaya, T.; Matsui, T.; Fujita, D.; Tosa, M.; Kondo, M.; Kitamori, T. Photocatalytic Generation of Hydrogen by Core-Shell $WO_3/BiVO_4$ Nanorods with Ultimate Water Splitting Efficiency. *Sci. Rep.* **2015**, *5*, 1−2.
(32) Chen, S.; Huang, D.; Xu, P.; Xue, W.; Lei, L.; Cheng, M.; Wang, R.; Liu, X.; Deng, R. *Semiconductor-Based Photocatalysts for Photocatalytic and Photoelectrochemical Water Splitting: Will We Stop with Photocorrosion?*; Royal Society of Chemistry, 2020; Vol. *8*, 2286. DOI: 10.1039/c9ta12799b.
(33) Yuan, N.; Jiang, Q.; Li, J.; Tang, J. A Review on Non-Noble Metal Based Electrocatalysis for the Oxygen Evolution Reaction. *Arabian J. Chem.* **2020**, *13*, 4294−4309.

(34) Wu, Z.-P.; Lu, X. F.; Zang, S.-Q.; Lou, X. W. (. D.). Non-Noble-Metal-Based Electrocatalysts toward the Oxygen Evolution Reaction. *Adv. Funct. Mater.* **2020**, *30*, 1910274.
(35) Xu, D.; Xia, T.; Fan, W.; Bai, H.; Ding, J.; Mao, B.; Shi, W. MOF-Derived Co_3O_4 Thin Film Decorated $BiVO_4$ for Enhancement of Photoelectrochemical Water Splitting. *Appl. Surf. Sci.* **2019**, *491*, 497−504.
(36) She, H.; Yue, P.; Huang, J.; Wang, L.; Wang, Q. One-Step Hydrothermal Deposition of F:FeOOH onto $BiVO_4$ Photoanode for Enhanced Water Oxidation. *Chem. Eng. J.* **2020**, *392*, No. 123703.
(37) Zhong, M.; Hisatomi, T.; Kuang, Y.; Zhao, J.; Liu, M.; Iwase, A.; Jia, Q.; Nishiyama, H.; Minegishi, T.; Nakabayashi, M.; Shibata, N.; Niishiro, R.; Katayama, C.; Shibano, H.; Katayama, M.; Kudo, A.; Yamada, T.; Domen, K. Surface Modification of CoO_x Loaded $BiVO_4$ Photoanodes with Ultrathin P-Type NiO Layers for Improved Solar Water Oxidation. *J. Am. Chem. Soc.* **2015**, *137*, 5053−5060.
(38) Irani, R.; Plate, P.; Höhn, C.; Bogdanoff, P.; Wollgarten, M.; Höflich, K.; Van De Krol, R.; Abdi, F. F. The Role of Ultra-Thin MnO_X Co-Catalysts on the Photoelectrochemical Properties of $BiVO_4$ Photoanodes. *J. Mater. Chem. A* **2020**, *8*, 5508−5516.
(39) Zhang, B.; Wang, L.; Zhang, Y.; Ding, Y.; Bi, Y. Ultrathin FeOOH Nanolayers with Abundant Oxygen Vacancies on $BiVO_4$ Photoanodes for Efficient Water Oxidation. *Angew. Chem., Int. Ed.* **2018**, *57*, 2248−2252.
(40) Luo, H.; Liu, C.; Xu, Y.; Zhang, C.; Wang, W.; Chen, Z. An Ultra-Thin NiOOH Layer Loading on $BiVO_4$ Photoanode for Highly Efficient Photoelectrochemical Water Oxidation. *Int. J. Hydrogen Energy* **2019**, *44*, 30160−30170.
(41) Zhang, J.; Huang, Y.; Lu, X.; Yang, J.; Tong, Y. Enhanced BiVO4Photoanode Photoelectrochemical Performance via Borate Treatment and a NiFeOx Cocatalyst. *ACS Sustainable Chem. Eng.* **2021**, *9*, 8306−8314.
(42) Du, J.; Zhong, X.; He, H.; Huang, J.; Yang, M.; Ke, G.; Wang, J.; Zhou, Y.; Dong, F.; Ren, Q.; Bian, L. Enhanced Photoelectrochemical Water Oxidation Performance on $BiVO_4$ by Coupling of $CoMoO_4$ as a Hole-Transfer and Conversion Cocatalyst. *ACS Appl. Mater. Interfaces* **2018**, *10*, 42207−42216.
(43) Fang, G.; Liu, Z.; Han, C. Enhancing the PEC Water Splitting Performance of BiVO4 Co-Modifying with NiFeOOH and Co-Pi Double Layer Cocatalysts. *Appl. Surf. Sci.* **2020**, *515*, No. 146095.
(44) Nellist, M. R.; Qiu, J.; Laskowski, F. A. L.; Toma, F. M.; Boettcher, S. W. Potential-Sensing Electrochemical AFM Shows CoPi as a Hole Collector and Oxygen Evolution Catalyst on $BiVO_4$ Water-Splitting Photoanodes. *ACS Energy Lett.* **2018**, *3*, 2286−2291.
(45) Lu, Y.; Su, J.; Shi, J.; Zhou, D. Surface Recombination Passivation of the BiVO4Photoanode by the Synergistic Effect of the Cobalt/Nickel Sulfide Cocatalyst. *ACS Appl. Energy Mater.* **2020**, *3*, 9089−9097.
(46) She, H.; Jiang, M.; Yue, P.; Huang, J.; Wang, L.; Li, J.; Zhu, G.; Wang, Q. Metal (Ni 2+ /Co 2+) Sulfides Modified BiVO 4 for Effective Improvement in Photoelectrochemical Water Splitting. *J. Colloid Interface Sci.* **2019**, *549*, 80−88.
(47) Tan, T.; Han, P.; Cong, H.; Cheng, G.; Luo, W. An Amorphous Cobalt Borate Nanosheet-Coated Cobalt Boride Hybrid for Highly Efficient Alkaline Water Oxidation Reaction. *ACS Sustainable Chem. Eng.* **2019**, *7*, 5620−5625.
(48) Wang, N.; Xu, A.; Ou, P.; Hung, S. F.; Ozden, A.; Lu, Y. R.; Abed, J.; Wang, Z.; Yan, Y.; Sun, M. J.; Xia, Y.; Han, M.; Han, J.; Yao, K.; Wu, F. Y.; Chen, P. H.; Vomiero, A.; Seifitokaldani, A.; Sun, X.; Sinton, D.; Liu, Y.; Sargent, E. H.; Liang, H. Boride-Derived Oxygen-Evolution Catalysts. *Nat. Commun.* **2021**, *12*, 6089.
(49) Jiang, W.-J.; Niu, S.; Tang, T.; Zhang, Q.-H.; Liu, X.-Z.; Zhang, Y.; Chen, Y.-Y.; Li, J.-H.; Gu, L.; Wan, L.-J.; Hu, J.-S. Crystallinity-Modulated Electrocatalytic Activity of a Nickel(II) Borate Thin Layer on Ni3B for Efficient Water Oxidation. *Angew. Chem., Int. Ed.* **2017**, *56*, 6572−6577.
(50) Gupta, S.; Patel, M. K.; Miotello, A.; Patel, N. Metal Boride-Based Catalysts for Electrochemical Water-Splitting: A Review. *Adv. Funct. Mater.* **2020**, *30*, 1906481.
(51) Turhan, E. A.; Nune, S. V. K.; Ülker, E.; Şahin, U.; Dede, Y.; Karadas, F. Water Oxidation Electrocatalysis with a Cobalt-Borate-Based Hybrid System under Neutral Conditions. *Chem. - Eur. J.* **2018**, *24*, 10372−10382.
(52) Xu, H.; Fan, W.; Zhao, Y.; Chen, B.; Gao, Y.; Chen, X.; Xu, D.; Shi, W. Amorphous Iron (III)-Borate Decorated Electrochemically Treated-BiVO4 Photoanode for Efficient Photoelectrochemical Water Splitting. *Chem. Eng. J.* **2021**, *411*, No. 128480.
(53) Kumar, S.; Satpati, A. K. Investigation of Interfacial Charge Transfer Kinetics of Photocharged Co-Bi Modified BiVO4 Using Scanning Electrochemical Microscopy (SECM). *Electrochim. Acta* **2021**, *368*, No. 137565.
(54) Kang, Z.; Lv, X.; Sun, Z.; Wang, S.; Zheng, Y. Z.; Tao, X. Borate and Iron Hydroxide Co-Modified BiVO4 Photoanodes for High-Performance Photoelectrochemical Water Oxidation. *Chem. Eng. J.* **2021**, *421*, No. 129819.
(55) Choi, S. K.; Choi, W.; Park, H. Solar Water Oxidation Using Nickel-Borate Coupled $BiVO_4$ Photoelectrodes. *Phys. Chem. Chem. Phys.* **2013**, *15*, 6499−6507.
(56) Xue, D.; Kan, M.; Qian, X.; Zhao, Y. A Tandem Water Splitting Cell Based on Nanoporous $BiVO_4$ Photoanode Cocatalyzed by Ultrasmall Cobalt Borate Sandwiched with Conformal TiO_2 Layers. *ACS Sustainable Chem. Eng.* **2018**, *6*, 16228−16234.
(57) Yang, L.; Liu, D.; Hao, S.; Kong, R.; Asiri, A. M.; Zhang, C.; Sun, X. A Cobalt-Borate Nanosheet Array: An Efficient and Durable Non-Noble-Metal Electrocatalyst for Water Oxidation at near Neutral PH. *J. Mater. Chem. A* **2017**, *5*, 7305−7308.
(58) Dastafkan, K.; Li, Y.; Zeng, Y.; Han, L.; Zhao, C. Enhanced Surface Wettability and Innate Activity of an Iron Borate Catalyst for Efficient Oxygen Evolution and Gas Bubble Detachment. *J. Mater. Chem. A* **2019**, *7*, 15252−15261.
(59) Wang, L.; Su, J.; Guo, L. Hierarchical Growth of a Novel Mn-Bi Coupled BiVO4 Arrays for Enhanced Photoelectrochemical Water Splitting. *Nano Res.* **2019**, *12*, 575−580.
(60) Liu, J.; Chen, T.; Juan, P.; Peng, W.; Li, Y.; Zhang, F.; Fan, X. Hierarchical Cobalt Borate/MXenes Hybrid with Extraordinary Electrocatalytic Performance in Oxygen Evolution Reaction. *ChemSusChem* **2018**, *11*, 3758−3765.
(61) Chen, P.; Xu, K.; Zhou, T.; Tong, Y.; Wu, J.; Cheng, H.; Lu, X.; Ding, H.; Wu, C.; Xie, Y. Strong-Coupled Cobalt Borate Nanosheets/Graphene Hybrid as Electrocatalyst for Water Oxidation Under Both Alkaline and Neutral Conditions. *Angew. Chem., Int. Ed.* **2016**, *55*, 2488−2492.
(62) Hu, Q.; Li, G.; Han, Z.; Wang, Z.; Huang, X.; Chai, X.; Zhang, Q.; Liu, J.; He, C. General Synthesis of Ultrathin Metal Borate Nanomeshes Enabled by 3D Bark-Like N-Doped Carbon for Electrocatalysis. *Adv. Energy Mater.* **2019**, *9*, 1901130.
(63) Hu, Y.; Wang, S.; Chen, P.; Yun, J.-H.; Hu, Y.; Ang, L. W. An Electrochemically Treated $BiVO_4$ Photoanode for Efficient Photoelectrochemical Water Splitting. *Angew. Chem., Int. Ed.* **2017**, *129*, 8620−8624.
(64) Ding, C.; Shi, J.; Wang, D.; Wang, Z.; Wang, N.; Liu, G.; Xiong, F.; Li, C. Visible Light Driven Overall Water Splitting Using Cocatalyst/$BiVO_4$ Photoanode with Minimized Bias. *Phys. Chem. Chem. Phys.* **2013**, *15*, 4589−4595.
(65) Glavee, G. N.; Klabunde, K. J.; Sorensen, C. M.; Hadjipanayis, G. C. Borohydride Reduction of Cobalt Ions in Water. Chemistry Leading to Nanoscale Metal, Boride, or Borate Particles. *Langmuir* **1993**, *9*, 162−169.
(66) Glavee, G. N.; Klabunde, K. J.; Sorensen, C. M.; Hadjapanayis, G. C. Borohydride Reductions of Metal Ions. A New Understanding of the Chemistry Leading to Nanoscale Particles of Metals, Borides, and Metal Borates. *Langmuir* **1992**, *8*, 771−773.
(67) Ozerova, A. M.; Simagina, V. I.; Komova, O. V.; Netskina, O. V.; Odegova, G. V.; Bulavchenko, O. A.; Rudina, N. A. Cobalt Borate Catalysts for Hydrogen Production via Hydrolysis of Sodium Borohydride. *J. Alloys Compd.* **2012**, *513*, 266−272.
(68) Nsanzimana, J. M. V.; Gong, L.; Dangol, R.; Reddu, V.; Jose, V.; Xia, B. Y.; Yan, Q.; Lee, J. M.; Wang, X. Tailoring of Metal Boride

https://doi.org/10.1021/acsomega.3c00104
ACS Omega 2023, 8, 20332−20341

Morphology via Anion for Efficient Water Oxidation. 2019, *9*, 1901503, DOI: 10.1002/aenm.201901503.
(69) Masa, J.; Sinev, I.; Mistry, H.; Ventosa, E.; de la Mata, M.; Arbiol, J.; Muhler, M.; Roldan Cuenya, B.; Schuhmann, W. Ultrathin High Surface Area Nickel Boride (NixB) Nanosheets as Highly Efficient Electrocatalyst for Oxygen Evolution. *Adv. Energy Mater.* **2017**, *7*, 1700381.
(70) Xu, N.; Cao, G.; Chen, Z.; Kang, Q.; Dai, H.; Wang, P. Cobalt Nickel Boride as an Active Electrocatalyst for Water Splitting. *J. Mater. Chem. A* **2017**, *5*, 12379−12384.
(71) Yan, D.; Fu, X.; Shang, Z.; Liu, J.; Luo, H. A BiVO4 Film Photoanode with Re-Annealing Treatment and 2D Thin $Ti_3C_2T_X$ Flakes Decoration for Enhanced Photoelectrochemical Water Oxidation. *Chem. Eng. J.* **2019**, *361*, 853−861.
(72) Fang, W.; Fu, L.; Qin, A.; Lin, Y.; Xv, R. Highly Active and Self-Healing Co-Doped BiVO4Photoanode in Borate Buffer to Enhance Charge Separation and Water Oxidation Kinetics during Photo-electrochemical Water Splitting. *ACS Appl. Energy Mater.* **2022**, 6313.
(73) Zhang, S.; Ahmet, I.; Kim, S. H.; Kasian, O.; Mingers, A. M.; Schnell, P.; Kölbach, M.; Lim, J.; Fischer, A.; Mayrhofer, K. J. J.; Cherevko, S.; Gault, B.; Van De Krol, R.; Scheu, C. Different Photostability of BiVO4in Near-PH-Neutral Electrolytes. *ACS Appl. Energy Mater.* **2020**, *3*, 9523−9527.

https://doi.org/10.1021/acsomega.3c00104
ACS Omega 2023, 8, 20332−20341